Action potentials and amphetamine release antipsychotic drug from dopamine neuron synaptic VMAT vesicles

Kristal R. Tucker[a], Ethan R. Block[b], and Edwin S. Levitan[a,1]

[a]Department of Pharmacology and Chemical Biology, University of Pittsburgh School of Medicine, Pittsburgh, PA 15261; and [b]Department of Cell Biology, University of Pittsburgh School of Medicine, Pittsburgh, PA 15261

Edited by Robert H. Edwards, University of California, San Francisco, CA, and accepted by the Editorial Board July 2, 2015 (received for review February 23, 2015)

Based on lysotracker red imaging in cultured hippocampal neurons, antipsychotic drugs (APDs) were proposed to accumulate in synaptic vesicles by acidic trapping and to be released in response to action potentials. Because many APDs are dopamine (DA) D2 receptor (D2R) antagonists, such a mechanism would be particularly interesting if it operated in midbrain DA neurons. Here, the APD cyamemazine (CYAM) is visualized directly by two-photon microscopy in substantia nigra and striatum brain slices. CYAM accumulated slowly into puncta based on vacuolar H^+-ATPase activity and dispersed rapidly upon dissipating organelle pH gradients. Thus, CYAM is subject to acidic trapping and released upon deprotonation. In the striatum, Ca^{2+}-dependent reduction of the CYAM punctate signal was induced by depolarization or action potentials. Striatal CYAM overlapped with the dopamine transporter (DAT). Furthermore, parachloroamphetamine (pCA), acting via vesicular monoamine transporter (VMAT), and a charged VMAT, substrate 1-methyl-4-phenylpyridinium (MPP^+), reduced striatal CYAM. In vivo CYAM administration and in vitro experiments confirmed that clinically relevant CYAM concentrations result in vesicular accumulation and pCA-dependent release. These results show that some CYAM is in DA neuron VMAT vesicles and suggests a new drug interaction in which amphetamine induces CYAM deprotonation and release as a consequence of the H^+ countertransport by VMAT that accompanies vesicular uptake, but not by inducing exchange or acting as a weak base. Therefore, in the striatum, APDs are released with DA in response to action potentials and an amphetamine. This synaptic corelease is expected to enhance APD antagonism of D2Rs where and when dopaminergic transmission occurs.

multiphoton | VMAT | vesicular release | amphetamine | antiporter

Most antipsychotic drugs (APDs) are competitive dopamine (DA) D2 receptor (D2R) antagonists (1, 2). The standard view is that APDs, by being weak bases that are in equilibrium with an uncharged form, cross the blood–brain barrier to access extracellular receptor binding sites from the circulation. However, because APDs are weak bases, they have been proposed to accumulate also in acidic intracellular organelles by acidic trapping (i.e., the less abundant uncharged basic hydrophobic form enters organelles passively and then is protonated to become membrane-impermeant). This hypothesis was first explored by examining a D2 antagonist with a covalently added fluorophore and APD displacement of acridine orange (3). More recently, APDs were found to be released from brain tissue by depolarization, which is expected for any positively charged drug. However, follow-up experiments in hippocampal neuron cultures showed that APDs displace the acidophilic dye lysotracker red, implying there is overlap in intracellular distribution between APDs and lysotracker red. Furthermore, lysotracker red was found to accumulate in hippocampal neuron synaptic vesicles by acidic trapping without displacing native neurotransmitter and to be released in response to electrical stimulation. Thus, based on the assumptions that lysotracker red is a surrogate for APDs and that the depolarization-evoked increase in APD concentration in vivo is due to vesicular release, it was proposed that APDs accumulate in synaptic vesicles by acidic trapping and are released in response to action potentials by vesicle exocytosis (4). The finding of lysotracker red release by unidentified neurons in hippocampal cultures led us to consider directly monitoring a clinically used APD in a context relevant to its action.

First, we reasoned that the vesicle acidic trapping mechanism would be important in DA neurons because acidic trapping in vesicular monoamine transporter (VMAT) vesicles would ensure that concentrated APDs are coreleased with native DA to antagonize D2R activation precisely when and where needed (i.e., at active DA synapses). In this way, off-target effects would be minimized and drug efficacy enhanced. Second, we set out to identify an APD that could be imaged with multiphoton microscopy in the living brain slice. Here, the APD cyamemazine (Tercian; CYAM) is visualized directly by two-photon microscopy in substantia nigra and striatum slices. Based on this imaging, CYAM acidic trapping in DA neuron VMAT vesicles is established and effects of action potentials and an amphetamine on CYAM release from DA neurons are discovered.

Results

Two-Photon Excitation of CYAM. CYAM absorbs UV light and emits green-orange fluorescence, making it detectable by fluorescence microscopy (5). Furthermore, photooxidation of CYAM is reduced in biomimetic microenvironments (6), raising the

Significance

Antipsychotic drugs (APDs) are dopamine (DA) receptor antagonists, whose action has been hypothesized to be affected by acidic trapping in and release by synaptic vesicles. However, acidic trapping of APDs has not been detected directly. Therefore, multiphoton microscopy was used to image an APD directly in living brain slices containing DA neurons. The APD accumulated by acidic trapping, and in the striatum, it was selectively depleted from DA synaptic vesicles by an amphetamine. Action potentials evoked Ca^{2+}-dependent striatal APD depletion, suggesting release by vesicle exocytosis. Therefore, APDs concentrate by acidic trapping in DA synaptic vesicles so that these antagonists will be coreleased with the native transmitter when and where physiological and pharmacological stimuli evoke dopaminergic transmission.

Author contributions: K.R.T., E.R.B., and E.S.L. designed research; K.R.T. performed research; E.R.B. contributed new reagents/analytic tools; K.R.T. and E.S.L. analyzed data; and K.R.T. and E.S.L. wrote the paper.

The authors declare no conflict of interest.

This article is a PNAS Direct Submission. R.H.E. is a guest editor invited by the Editorial Board.

[1]To whom correspondence should be addressed. Email: elevitan@pitt.edu.

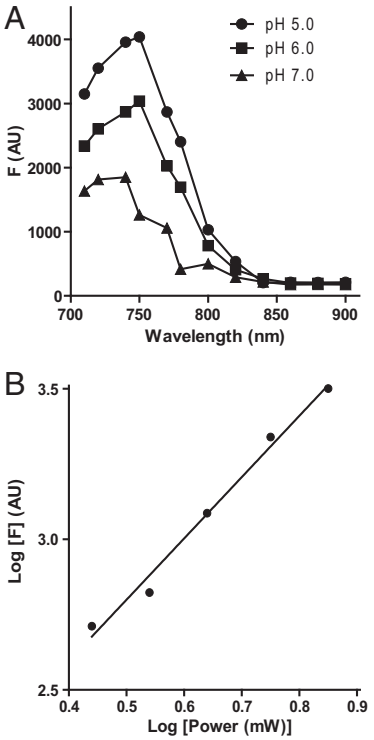

Fig. 1. Two-photon excitation of CYAM. (*A*) Multiphoton excitation spectrum of 2 mM CYAM in phosphate-citrate buffer at pH 5.0 (●), pH 6.0 (■), and pH 7.0 (▲). CYAM fluorescence was measured and background-subtracted at the indicated wavelengths and pH values. Data are not corrected for changes in laser output with wavelength. (*B*) Two-photon excitation of CYAM. CYAM (2 mM) in phosphate-citrate buffer at pH 5 was excited with increasing levels of power at 780 nm. Circles (●) indicate individual data points, and the line represents the linear regression through those points with a slope of 2.04. AU, arbitrary unit; F, fluorescence.

possibility of imaging CYAM in neurons. CYAM has a log P (partition coefficient) of 4.4 and a pK_a of 9.3, suggesting that it could act as a membrane-permeant weak base. Furthermore, in fibroblasts, CYAM colocalizes with lysotracker red, implying that this APD is subject to acidic trapping in lysosomes (5). Therefore, we explored whether CYAM could be detected with multiphoton microscopy, which would enable studying its distribution in living brain slices. In fact, illumination of CYAM in solution with near-IR excitation light from a titanium/sapphire laser produced visible fluorescence (Fig. 1*A*). This fluorescence showed modest pH sensitivity: In contrast to a standard pH curve, fluorescence changed linearly and only halved between pH 5 and pH 7 (Fig. 1*A*). A log fluorescence vs. log power plot had a slope of 2.0, implying that CYAM is subject to two-photon excitation (Fig. 1*B*).

Acidic Trapping in Brain Slices. We then examined CYAM accumulation in brain slices containing the substantia nigra pars compacta (SNc), a region containing many DA neuron somata, and the striatum, a region with many DA neuron terminals. Applying a protocol developed for studying hippocampal cultures (4) revealed widespread punctate accumulation of CYAM (Fig. 2*A*). Many features of this accumulation are consistent with acidic trapping. First, CYAM puncta appeared slowly over the period of an hour (Fig. 2 *A* and *B*). Second, inhibiting the vacuolar H^+-ATPase with bafilomycin A1 (Baf A) blocked the appearance of CYAM puncta (Fig. 3*A*). This result is expected because acidic trapping relies on the vacuolar H^+-ATPase maintaining luminal organelle acidity by replacing protons bound by the membrane-permeant unprotonated form of weak bases. In this way, slow acidic trapping of APDs can proceed without changing vesicular neurotransmitter content (4). Finally, applying ammonium chloride (NH_4Cl) to collapse organelle pH gradients, but not control saline (Cont), rapidly eliminated CYAM puncta in SNc (Fig. 3 *B* and *C*). A similar effect was seen in striatum (Str) slices (Fig. 3*D*), which contain many DA synaptic boutons. Notably, this elimination is essentially complete, and thus not explained by the modest pH sensitivity of CYAM intrinsic fluorescence. Therefore, CYAM must have dispersed following organelle deacidification and drug deprotonation. These results show that CYAM is subject to acidic trapping in the SNc and striatum and is readily released when organelle pH gradients are collapsed.

Activity and Amphetamine Do Not Release CYAM from the DA Neuron Soma. We then examined whether CYAM accumulates in the soma of SNc DA neurons. First, ovoid neurons were patch-clamped and filled with the far red dye Cy5, which can be distinguished from CYAM based on spectral differences (Fig. 4*A*). DA neurons were then identified based on the voltage sag produced by hyperpolarization, spontaneous pacemaker activity, and broad action potentials (Fig. 4*B*). In electrophysiologically identified DA neurons, punctate CYAM was detectable (Fig. 4*A*). To verify this result independently, CYAM-treated slices were imaged before and after incubation with IDT307 (also called APP^+), a fluorescent substrate of plasma membrane monoamine transporters (7–9). Because the DA transporter (DAT) is the only somatic monoamine transporter in the SNc, somatic IDT307 labeling identifies DA neurons. Based on IDT307 labeling, it was evident that CYAM accumulates in the DA neuron soma (Fig. 4*C*). Therefore, two independent approaches verified that CYAM puncta are present in the DA neuron soma.

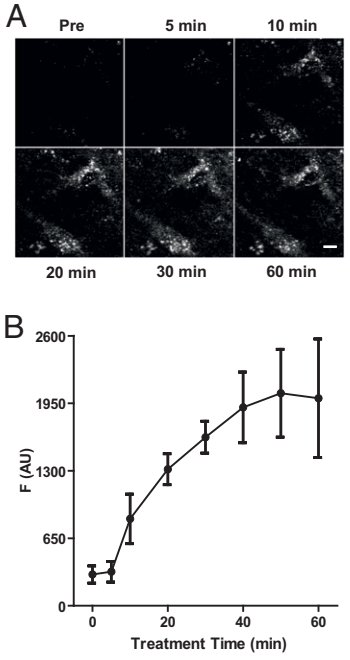

Fig. 2. CYAM slowly accumulates into puncta in the SNc brain slice. (*A*) 2P images of CYAM fluorescence in the SNc of a midbrain slice before (Pre) and after 5, 10, 20, 30, and 60 min of 5 μM CYAM treatment at 37 °C. (Scale bar: 5 μm.) (*B*) Quantification of CYAM accumulation. Fluorescence from a 60 × 60-μm ROI expressed in arbitrary units was measured at the indicated time points. Circles (●) and error bars represent the mean and SEM of three experiments.

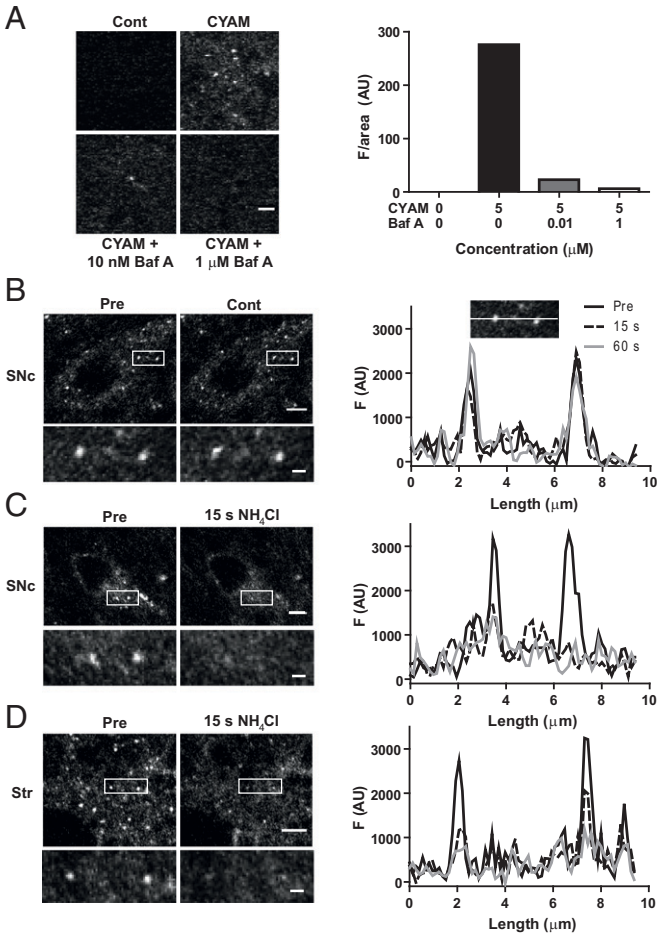

Fig. 3. Acidic trapping of CYAM. (*A*) CYAM accumulation in the presence of Baf A. 2P images (*Left*) and quantification of CYAM fluorescence (*Right*) in dorsolateral striatum slices pretreated for 30 min with aCSF, 10 nM Baf A, or 1 μM Baf A and then coincubated with CYAM or aCSF [control (Cont)] for 1 h. (*Right*) Bars indicate mean CYAM fluorescence for two experiments. (Scale bar: 2 μm.) (*B–D*, Left) 2P images of CYAM fluorescence in SNc (*B* and *C*, *Left*) and striatum (Str; *D*, *Left*) slices before and after 5 mM NH_4Cl (*C* and *D*, *Left*) or time-matched vehicle control (*B*, *Left*). The white box in each image indicates the region enlarged beneath. (Scale bars: whole image, 5 μm; enlarged image, 1 μm.) (*B–D*, *Right*) Profile plots of punctate fluorescence (*Right*) in the enlarged images (*Left*) are shown. (*B*, *Right Inset*) Example of where the fluorescence measurements for the profile plots were taken for the Pre, 15-s, and 60-s time points.

Acidic VMAT vesicles mediate DA release from terminals and dendrites, but these vesicles have not been extensively studied in the soma. Therefore, DA neurons were stimulated by depolarization with bath-applied 50 mM KCl. However, no change in CYAM fluorescence was observed in the presence or absence of Ca^{2+} (Fig. 5 *A* and *B*). Likewise, inducing action potentials at 10 Hz for 2 min in patch-clamped DA neurons also failed to elicit a CYAM response (Fig. 5 *C* and *D*). Moreover, parachloroamphetamine (pCA), an amphetamine known to act at both plasma membrane transporter and VMAT to release DA and serotonin (10), had no significant effect on CYAM fluorescence in IDT307-positive somas of the SNc (5.5 ± 4.8%; $n = 6$; $P = 0.35$). Therefore, CYAM in the DA neuron soma is not released by activity or amphetamine.

Activity-Dependent CYAM Responses in the Striatum. CYAM puncta were then studied in striatum slices, where there is an abundance of DA terminals. First, in contrast to controls, depolarization with 50 mM K^+ evoked a decrease in punctate CYAM fluorescence (Fig. 6 *A* and *B*). Consistent with vesicle exocytosis, this effect was inhibited by either removing extracellular Ca^{2+} or supplementing the saline with 200 μM Cd^{2+}, a Ca^{2+} channel blocker (Fig. 6 *A* and *B*). Second, 10-Hz field stimulation also evoked a CYAM response (Fig. 6 *C* and *D*). Interestingly, the 10% decrease in mean fluorescence is comparable to the decrease found using similar stimulation in the striatum with the false fluorescent neurotransmitter FFN102 before separating responders from nonresponders (11). Again, removing Ca^{2+} was inhibitory. Furthermore, the sodium channel blocker tetrodotoxin (TTX) abolished the response to field stimulation, showing that action potentials are necessary (Fig. 6 *C* and *D*). Together, these results suggest that action potentials evoke Ca^{2+}-dependent vesicular release of CYAM in the striatum.

Amphetamine-Induced CYAM Responses in Striatum Slices. To determine whether CYAM could be present in DA endings, the APD and DAT were localized in the striatum slice. Two approaches were used. First, CYAM and IDT307 were imaged. IDT307 labeling was not punctate like CYAM, because this DAT substrate fills DA neuron processes but likely does not get packaged into vesicles (8). Importantly, punctate CYAM fluorescence was present in IDT307-labeled structures (Fig. 7*A*). Second, HA-tagged DAT was detected by immunofluorescence in striatum slices from knock-in mice (12). Again, there was overlap of DAT and CYAM (Fig. 7*B*). These two experiments suggest that some of the detected CYAM in the striatum is associated with DA neurons. However, optical microscopy cannot resolve whether CYAM is actually inside DA neurons.

Therefore, we took advantage of the facts that amphetamines are substrates for plasma membrane transporters [e.g., DAT, serotonin transporter (SERT)] (10, 13) and can reduce the vesicular pH gradient (14). Because the latter effect would be expected to counter acidic trapping, the effect of pCA was studied. Notably, 20 μM and 100 μM pCA lowered the average signal from striatal CYAM puncta (Fig. 8 *A* and *B*). This result does not exclude the possibility that pCA enters organelles passively to act by a weak base mechanism to decrease CYAM fluorescence. Therefore, we examined the effect of applying 500 nM reserpine to the slice, which effectively inhibits VMAT (15), just before pCA. With 100 μM pCA, reserpine had no effect, but reserpine inhibited the response to 20 μM pCA. Furthermore, striatal cells that had no monoamine transporters, which were identified based on lack of IDT307 labeling, failed to respond to 20 μM pCA but responded to 100 μM pCA (Fig. 8 *C* and *D*). Together, these experimental results show that 100 μM pCA acts as a simple weak base. However, 20 μM pCA requires VMAT to affect CYAM.

The reserpine effect at the lower pCA concentration could arise from DA and serotonin terminals in the dorsal striatum because both possess VMAT. Therefore, to determine whether pCA acted selectively in DA and/or serotonin neurons, DAT was inhibited with 10 μM GBR 12909 or 1 μM nomifensine and SERT was inhibited with 10 μM fluoxetine (Fig. 8 *E* and *F*). Upon inhibiting DAT-mediated uptake, pCA action was blocked. In contrast, inhibiting SERT had no effect. Moreover, GBR 12909, nomifensine, and fluoxetine had no significant effect on CYAM fluorescence in the absence of pCA. Together, these results show that widespread CYAM acidic trapping includes presynaptic DA vesicles from which the APD can be specifically depleted by an amphetamine.

Mechanism of Amphetamine-Induced CYAM Release. We then examined the VMAT-dependent mechanism mediating APD release by the lower concentration of pCA. Amphetamines are VMAT substrates and can induce DA release from DA-containing vesicles either by acting as weak bases to reduce the vesicular pH gradient

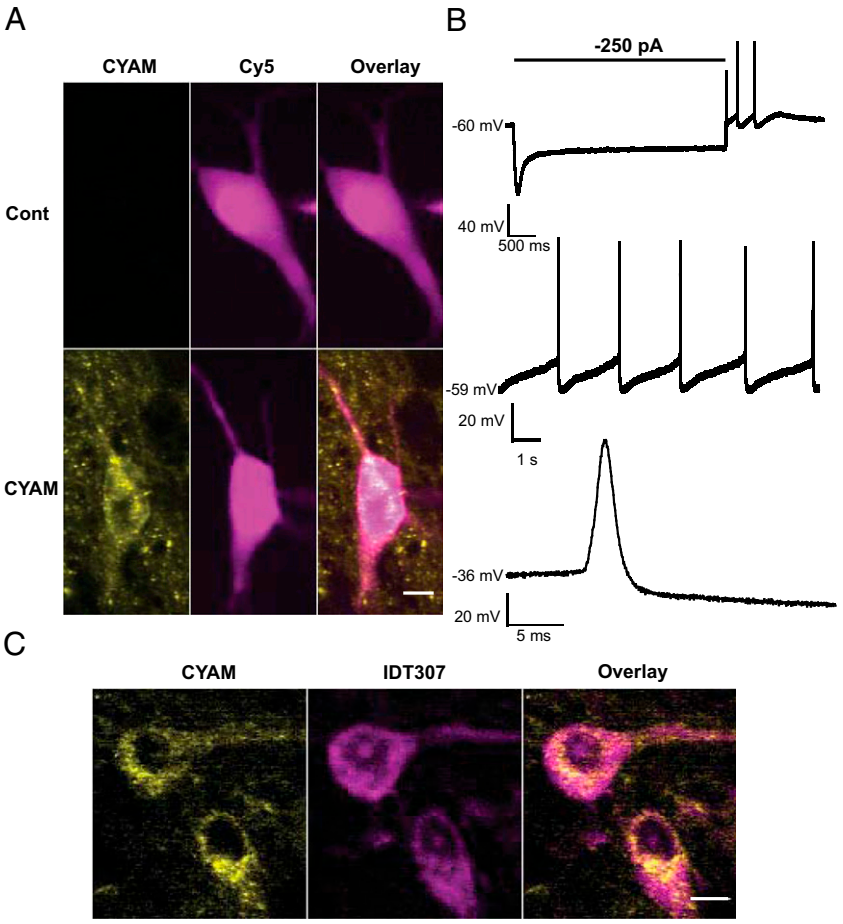

Fig. 4. CYAM in SNc DA neurons. (*A*, *B*) Electrophysiological confirmation of SN DA neuron CYAM accumulation. During whole-cell patch-clamp recordings, cells from control and CYAM-treated slices were filled with patch-pipette solution containing 10 μM sulfo-Cy5-COOH (Cy5). (*A*) Pseudocolored summed z-projections of CYAM (yellow) and Cy5 (magenta) fluorescence signals. (Scale bar: 10 μm.) (*B*) Representative current-clamp voltage traces of electrophysiological characteristics used to establish dopaminergic identity of a cell. (*Top*) Characteristic Ih voltage sag and spontaneous rebound spiking activity of a neuron that was current-clamped at −60 mV, followed by a 4-s, −250-pA current injection. Slow pacemaker activity (*Middle*) and broad action potentials (*Bottom*) are characteristic of SNc DA neurons. (*C*) Colocalization of CYAM (yellow) and two monoamine neurons in the SNc identified with IDT307 (magenta). (Scale bar: 10 μm.)

or by inducing VMAT-mediated exchange with luminal DA (14–19). VMAT-mediated exchange can only occur with two VMAT substrate molecules (20). Therefore, to test whether exchange could occur with CYAM, the effect of the VMAT inhibitor reserpine on punctate accumulation of CYAM in the striatum was determined. Application of reserpine before CYAM did not affect CYAM accumulation into puncta in the striatum (Fig. 9*A*). Thus, CYAM accumulates without the involvement of VMAT. This result is expected for acidic trapping and is consistent with CYAM accumulation in nonmonoaminergic cells (example in Fig. 8*C*). Therefore, as expected, there is no indication that CYAM is a VMAT substrate. This finding implies that the pCA effect cannot be explained by VMAT-mediated exchange of pCA for CYAM.

Therefore, the possibility that VMAT promotes the entry of uncharged pCA to enhance the weak base effect was examined. This hypothesis predicts that a permanently charged VMAT substrate, which therefore cannot act as a base, would not affect accumulated CYAM. However, 50 μM 1-methyl-4-phenylpyridinium (MPP^+) decreased CYAM in the striatum (Fig. 9*B*). This result rules out a facilitated weak base mechanism. Given that an exchange mechanism was also excluded, the MPP^+ result favors an alternative model in which uptake of substrates by VMAT, which is associated with proton countertransport, displaces the APD from the DA vesicle (*Discussion*).

CYAM Responses at Nanomolar Concentrations and Following in Vivo Dosing. The results discussed above were obtained after incubating slices with 5 μM CYAM for an hour. Therefore, we assessed whether accumulation could be detected at the lower concentrations that are more likely to be encountered clinically. For detection, micromolar CYAM was required with the 1-h incubation. However, with a 3-h incubation, CYAM accumulation in striatum slices was detectable even at 5 nM, which is approaching the affinity for the drug for D2Rs (Fig. 10 *A* and *B*). Furthermore, 20 μM pCA reduced the 5 nM CYAM signal (Fig. 10*C*). Thus, acidic trapping and amphetamine-induced release are still evident after reducing the CYAM concentration 1,000-fold. These results led us to explore whether slices isolated in the absence of added drug yielded a detectable CYAM signal after in vivo administration. Consistent with the known slow onset of clinical efficacy of APDs, a 2.5-mg/kg dose administered twice daily for 5 d (120 h) yielded detectable CYAM in striatal slices (Fig. 10 *D* and *E*). Furthermore, subsequent application of 20 μM pCA elicited a CYAM response (Fig. 10*F*). These results obtained with low concentrations in in vitro and in vivo dosing demonstrate that CYAM accumulation in DA vesicles is not an artifact of high concentrations or direct application to slices. Therefore, together with the effects of amphetamine, action potentials, DAT inhibitors, reserpine, and MPP^+, these results imply that synaptic DA vesicle exocytosis or amphetamines will result in corelease of DA and concentrated trapped APD.

Discussion

This study reports the direct optical imaging of a clinically relevant psychiatric drug in a living brain slice. First, multiphoton microscopy in the SNc and striatum establish that the APD CYAM accumulates by acidic trapping. Furthermore, the organelle CYAM pool was found to respond to action potentials in the striatum. Thus, drug released in response to synaptic activity by many neurons may contribute to the ongoing blockade of D2Rs by APDs. Because optical measurements also demonstrated acidic

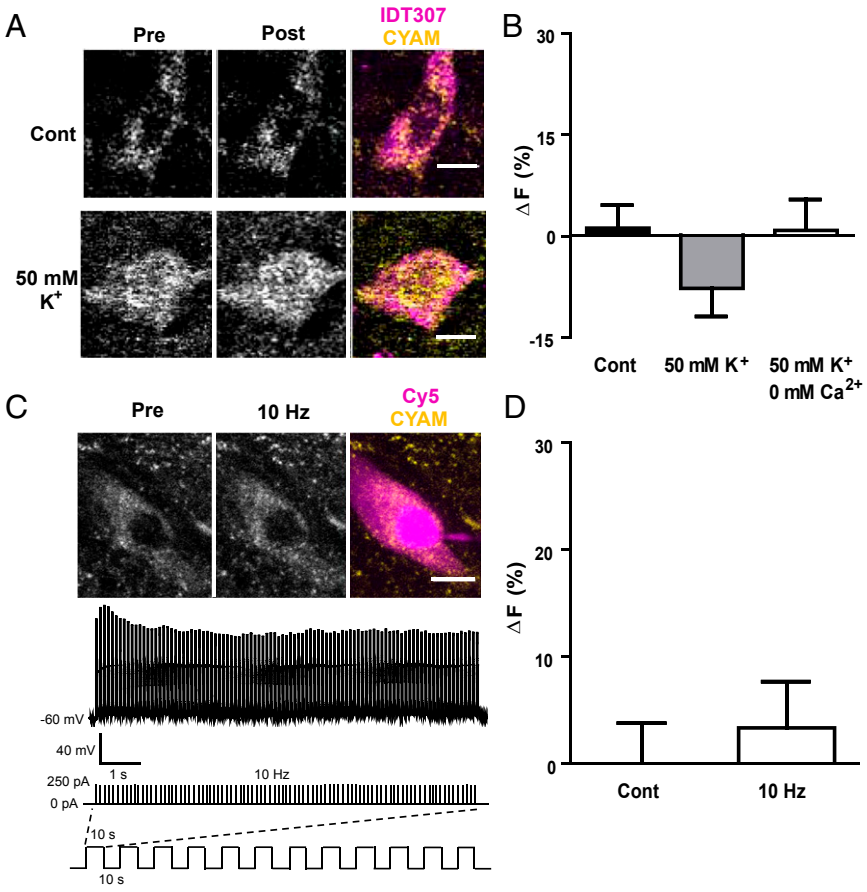

Fig. 5. Acute depolarization and activity do not affect somatic CYAM in DA neurons. 2P images (*A*) and quantification of CYAM fluorescence change (*B*; ΔF) in SNc IDT307-positive soma before and 2 min after (Post) treatment with aCSF (control; $n = 13$), 50 mM K^+ aCSF (50 mM K^+; $n = 18$), and 0 mM Ca^{2+}/50 mM K^+ aCSF (*B* only; $n = 5$). IDT307 (magenta) and CYAM (yellow) fluorescence colocalization is shown in the pseudocolored overlay in *A*. Note that release would produce a positive value for ΔF, not the statistically insignificant negative value seen here. (*C*) Electrophysiologically identified CYAM containing SNc DA neurons as described in Fig. 4 *A* and *B* were electrically stimulated via patch pipette with twelve 10-s-long bouts every 10 s at a frequency of 10 Hz as depicted in the schematic at the bottom of *C*. Each 10-s, 10-Hz stimulation bout resulted in a train of action potentials as shown in the voltage trace in *C*. Representative 2P image (*C*, *Top*) and quantification of the change in CYAM fluorescence (*D*; ΔF) in unstimulated (control; $n = 12$) and electrically stimulated (10 Hz; $n = 8$) SNc DA neurons. The patched cell is indicated in the pseudocolored overlay with the intracellular CY5 fill in magenta and the CYAM fluorescence in yellow. Bars represent mean ± SEM. (Scale bars: *A* and *C*, 10 μm.)

trapping in DA neuron VMAT vesicles, these experiments suggest that the efficacy of APDs could be especially enhanced by synaptic corelease with DA. Specifically, corelease would ensure that the D2R antagonist is present in the synaptic cleft when and where DA transmission occurs. Given limitations in on-rate and the preferential clearance of DA, but not APDs, we propose that synaptic vesicle APDs may be particularly effective following bursts of DA neuron activity, which are thought to be important for behavior (21). Furthermore, CYAM and DA can be coreleased in response to amphetamine. Therefore, acidic trapping of the APD promotes D2R antagonism at active sites of physiologically or pharmacologically induced DA release but, otherwise, retains APDs to reduce off-target effects.

Interestingly, the effect of the lower concentration of amphetamine on vesicular APD is not accounted for by two common models (i.e., vesicle deacidification by a weak base effect, VMAT-mediated exchange with no net proton flux) (16, 19, 22). First, if pCA-mediated CYAM release were merely a result of unprotonated pCA passively entering into the cell and vesicles, this effect would be independent of monoamine transporters and would occur in all cells. This independence appears to be the case with 100 μM pCA, but at 20 μM, pCA was sensitive to inhibiting DAT or VMAT and did not alter CYAM in cells devoid of plasma membrane monoamine transporters. Furthermore, MPP^+, which is not a weak base, evoked a comparable CYAM response. Therefore, although the amphetamine at a very high concentration works as a weak base, at the lower concentration, the amphetamine must enter the cell via DAT and then the vesicle through VMAT to induce CYAM release. Finally, consistent with fibroblast experiments (5), CYAM uptake is also not based on being a VMAT substrate, arguing against VMAT-mediated pCA-CYAM exchange and supporting acidic trapping as the mechanism for CYAM accumulation.

Because two prior models have been excluded for explaining the amphetamine effect, we suggest a mechanism based on the rapid dispersion of CYAM upon deprotonation (Fig. 3 *B* and *C*) and the function of VMAT, which transports two luminal protons out of the vesicle lumen for every monovalently charged substrate molecule transported into the vesicle (20). Because amphetamines are VMAT substrates, upon acute application, their transport into vesicles will produce countertransport of protons out of vesicles (i.e., because VMAT is a monoamine-proton antiporter). In this way, amphetamines are similar to tyramine, which can act both as a weak base and as a VMAT substrate that induces proton countertransport out of the vesicle (23, 24). The resultant efflux of protons will promote deprotonation of CYAM inside the vesicle, which, in turn, induces CYAM diffusion out of the vesicle. According to our model, the ability of unprotonated CYAM to leave the vesicle passively leads to a rapid buffering of luminal pH to limit engagement of slower vacuolar H^+-ATPase activity. The rapid and passive exit of CYAM contrasts with DA, whose VMAT-mediated efflux will be slowed by the interaction of luminal catecholamine with ATP, its greater hydrophilicity, and VMAT kinetics. Therefore, this model posits that amphetamine can induce different mechanisms to release CYAM and DA from vesicles. Indeed, this mechanism could be the basis of a novel interaction between weak base drugs and VMAT substrates.

Our experiments showed that Ca^{2+}-dependent CYAM responses were evoked by depolarization or action potentials in striatal terminals, but not in the SNc DA neuron soma. Similarly, amphetamine was effective in the striatum, but not in SNc DA neuron somata. The simplest interpretation of the depolarization and activity results is that somatic accumulation occurs in acidic

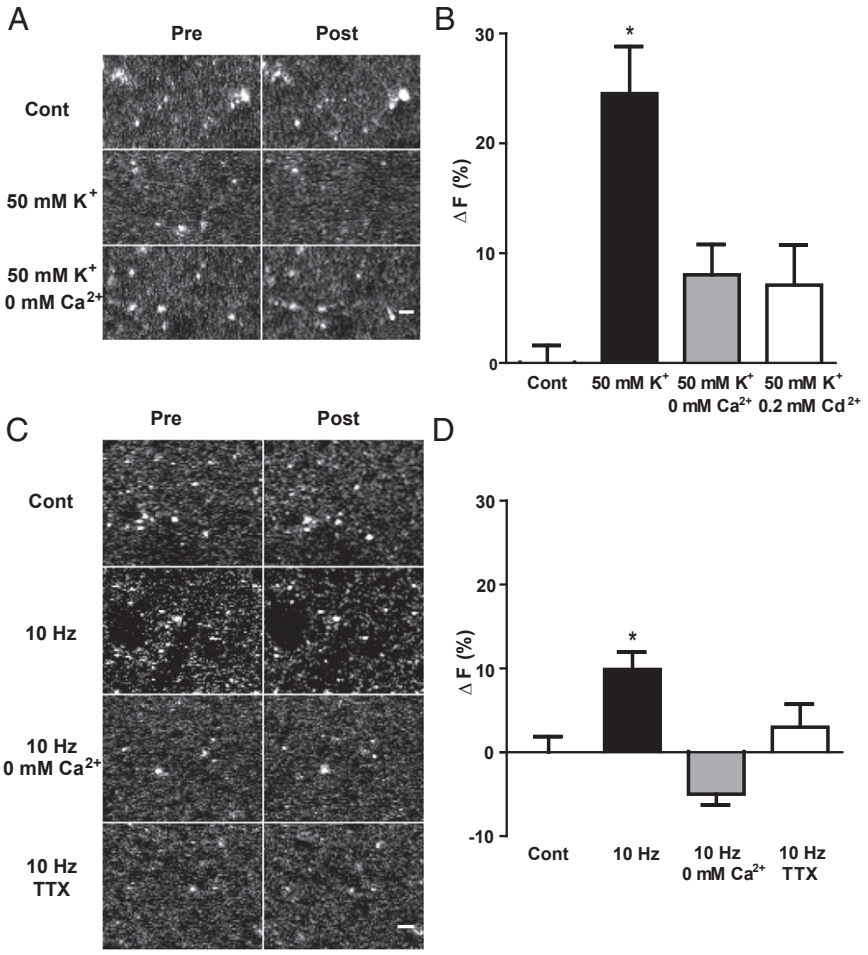

Fig. 6. Activity and depolarization evoke Ca^{2+}-dependent CYAM release in the striatum. 2P images (*A*) and quantification of the change in punctate CYAM fluorescence (*B*; ΔF) in striatum slices taken before and 2 min after treatment with aCSF (control; $n = 7$), 50 mM K^+ aCSF (50 mM K^+; $n = 8$), 50 mM K^+ aCSF without Ca^{2+} (50 mM K^+/0 mM Ca^{2+}; $n = 4$), or 50 mM K^+ aCSF with 0.2 mM Cd^{2+} (*B* only; 50 mM K^+/0.2 mM Cd^{2+}; $n = 5$). Representative 2P images (*C*) and quantification of the change in striatum CYAM fluorescence (*D*; ΔF) before and after field stimulation (10 Hz, 30 mA for 2 min) in time-matched control conditions without stimulation ($n = 11$), and 10-Hz stimulation in aCSF (10 Hz; $n = 16$), in aCSF without Ca^{2+} (10 Hz/0 mM Ca2$^+$; $n = 5$), and in aCSF with 1 μM TTX (10 Hz/TTX; $n = 8$). (Scale bars: *A* and *C*, 2 μm.) Bars represent mean ± SEM. $^*P < 0.05$.

organelles that are not competent for release (lysosomes, endosomes, and autophagosomes). Furthermore, pCA experiments suggest that VMAT-containing organelles in the soma are sparse, and therefore obscured by other acidic organelles or are not acidified. It is also possible that 20 min of pCA treatment was too short to detect a somatic CYAM response, because the false fluorescent neurotransmitter FFN102 is released from the soma of DA neurons only after 40 min of incubation with 1 μM amphetamine (11). Nevertheless, the region-specific differences in CYAM responses suggest that the soma, in contrast to terminals, is not optimized for vesicular release of DA and CYAM.

Acidic trapping of drugs in synaptic vesicles not only focuses when and where a drug is released but also affects the local concentration of APD upon release. In addition to being D2R antagonists, many APDs affect other targets at higher concentrations, including the ether-a-go-go–related gene potassium channel (ERG; reviewed in 25). Indeed, ERG potassium channel inhibition has been suggested to play a role in the efficacy of APDs because of its role in depolarization blockade (25, 26). Sodium channels are another low-affinity target of APDs that are implicated in DA neuron depolarization blockade (27). Therefore, localized concentrated activity-dependent vesicular release following acidic trapping could contribute to the noncanonical effects of APDs.

This study demonstrated the feasibility of imaging an unmodified clinically relevant drug in the living brain slice. By imaging CYAM with multiphoton microscopy, it was possible to observe drug distribution directly in the tissue and determine conditions for release. We found CYAM is sequestered by acidic trapping into acidic organelles in both the soma and axons of multiple neuron types, but most importantly for this D2R antagonist, it accumulates into synaptic VMAT vesicles of DA neurons and is released by activity and an amphetamine. Beyond their relevance for APDs, these studies establish the feasibility of

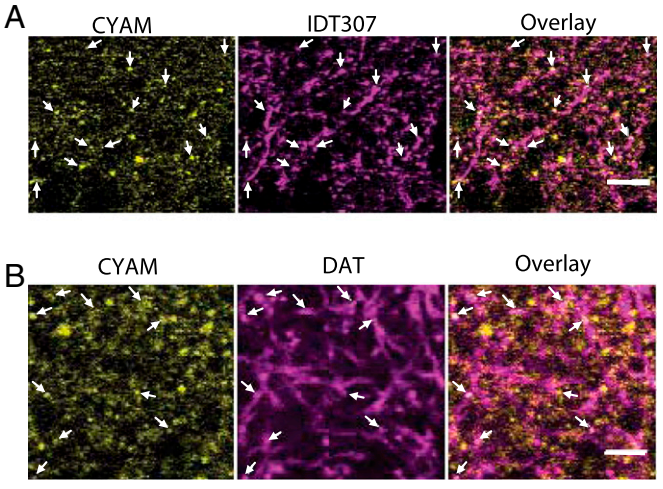

Fig. 7. CYAM accumulates in striatal DA endings. (*A*) 2P image from the striatum treated with CYAM (yellow), followed by incubation with IDT307 (magenta). (*B*) Confocal image of HA-DAT immunofluorescence (DAT; magenta) and 2P image of CYAM fluorescence (yellow) in striatum. White arrows indicate some areas of colocalization. (Scale bars: 5 μm.)

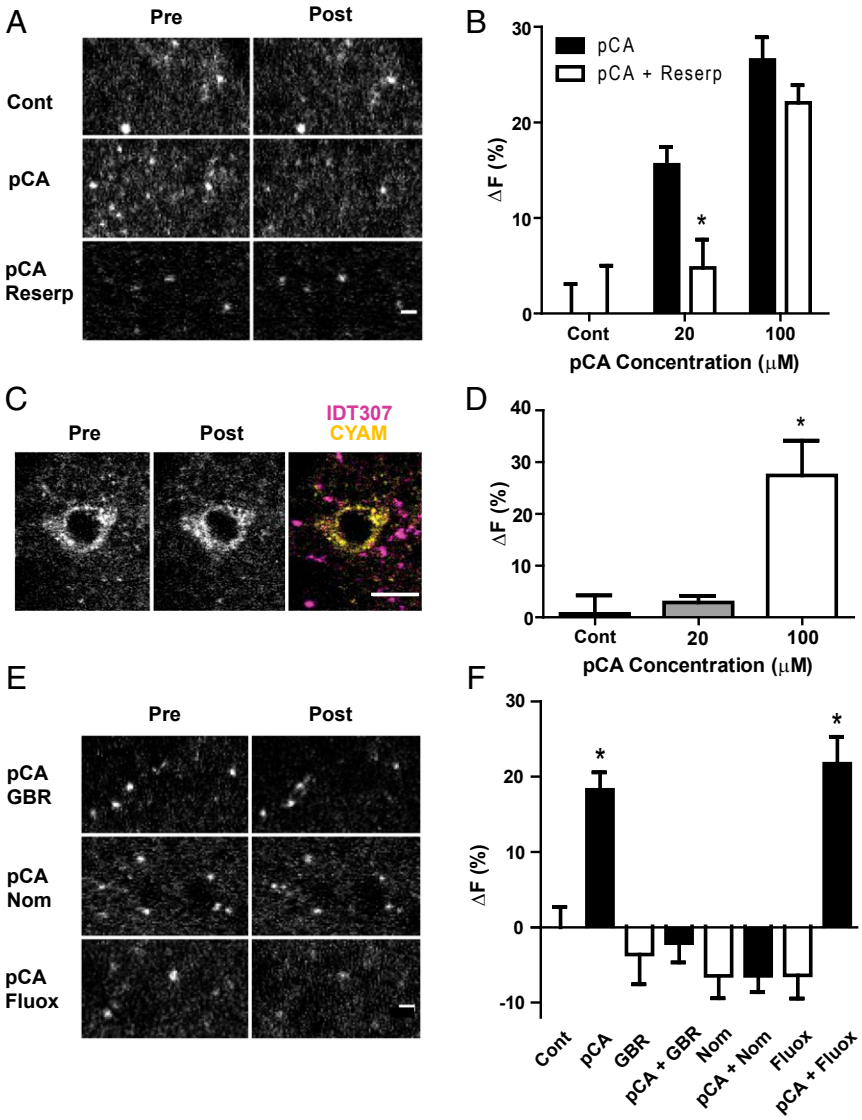

Fig. 8. pCA depletion of CYAM is VMAT-dependent and DAT-dependent, but not SERT-dependent. (*A* and *B*) Reserpine prevents changes in CYAM fluorescence with 20 μM but not 100 μM pCA. 2P images (*A*) and quantification of CYAM fluorescence (*B*) of CYAM-treated striatum slices preincubated for 30 min with 500 nM reserpine or vehicle control before a 20-min coincubation with 0, 20, or 100 μM pCA [pCA + reserpentine (Reserp)]. (Scale bar: 2 μm.) $*P < 0.05$ ± reserpine treatment. (*C* and *D*) pCA does not reduce CYAM fluorescence in nonmonoaminergic cells at VMAT selective doses. (*C*) 2P image of a CYAM-containing IDT307-negative (i.e., nonmonoaminergic) cell before and after 20-μm pCA treatment. (Scale bar: 10 μm.) (*D*) Quantification of change in CYAM fluorescence of nonmonoaminergic cells of the striatum in response to 0, 20, and 100 μM pCA ($n = 4$–5 cells per treatment). (*E* and *F*) To determine how much of the pCA effect is due to DA terminals, CYAM-treated striatum slices were preincubated with 10 μM GBR 12909 (GBR; DAT antagonist), 10 μM fluoxetine (Fluox; SERT antagonist), or 1 μM nomifensine (Nom; DAT and norepinephrine transporter antagonist) before coincubation with 20 μM pCA (black bars) or aCSF (white bars). 2P images (*E*) and quantification of the change in CYAM fluorescence (*F*) before and after pCA treatment as indicated. $*P < 0.05$ vs. control ($n = 3$–13 slices per treatment). (Scale bar: 2 μm.)

using multiphoton microscopy to image psychiatric and neurological drugs directly in the brain slice to study their mechanisms of action.

Materials and Methods

Slice Preparation. All experiments were conducted according to University of Pittsburgh Institutional Animal Care and Use Committee-approved protocols and National Institutes of Health guidelines. Postnatal day 13 male Sprague–Dawley rat pups and their mothers were obtained from Hilltop or Harlan Laboratories. Knock-in mice with an HA tag on the external surface of the DAT (HA-DAT) have been previously described (12). Rats and mice were housed in the University of Pittsburgh vivarium, maintained on a 12:12-h light/dark cycle, and had ad libitum access to food and water.

Midbrain slice preparations from both rat and HA-DAT mice were performed as previously described for rats (28), with the addition of including the striatum in the sectioning. In brief, postnatal day 14–28 male Sprague–Dawley rats or HA-DAT mice were anesthetized with isoflurane and decapitated. The brain was then quickly removed and placed into ice-cold, 95% O_2- and 5% (vol/vol) CO_2-saturated, sucrose-modified artificial cerebral spinal fluid (s-aCSF) containing the following: 87 mM NaCl, 75 mM sucrose, 2.5 mM KCl, 25 mM $NaHCO_3$, 1.25 mM NaH_2PO_4, 0.5 mM $CaCl_2$, 7 mM $MgSO_4$, 25 mM glucose, 0.15 mM ascorbic acid, and 1 mM kynurenic acid (pH 7.4). Coronal striatum and midbrain slices containing the SNc (250 μm) were cut using a Vibratome 3000 (The Vibratome Company) in ice-cold s-aCSF and then held in s-aCSF at room temperature for 30 min.

CYAM (Sigma–Aldrich) slice treatments were initially based on protocols used by Tischbirek et al. (4): Brain slices were treated for 1 h at 37 °C with 5 μM CYAM in 95% O_2- and 5% CO_2-saturated aCSF containing the following: 124 mM NaCl, 4 mM KCl, 25.7 mM $NaHCO_3$, 1.25 mM NaH_2PO_4, 2.45 mM $CaCl_2$, 1.2 mM $MgSO_4$, 11 mM glucose, and 0.15 mM ascorbic acid (pH 7.4).

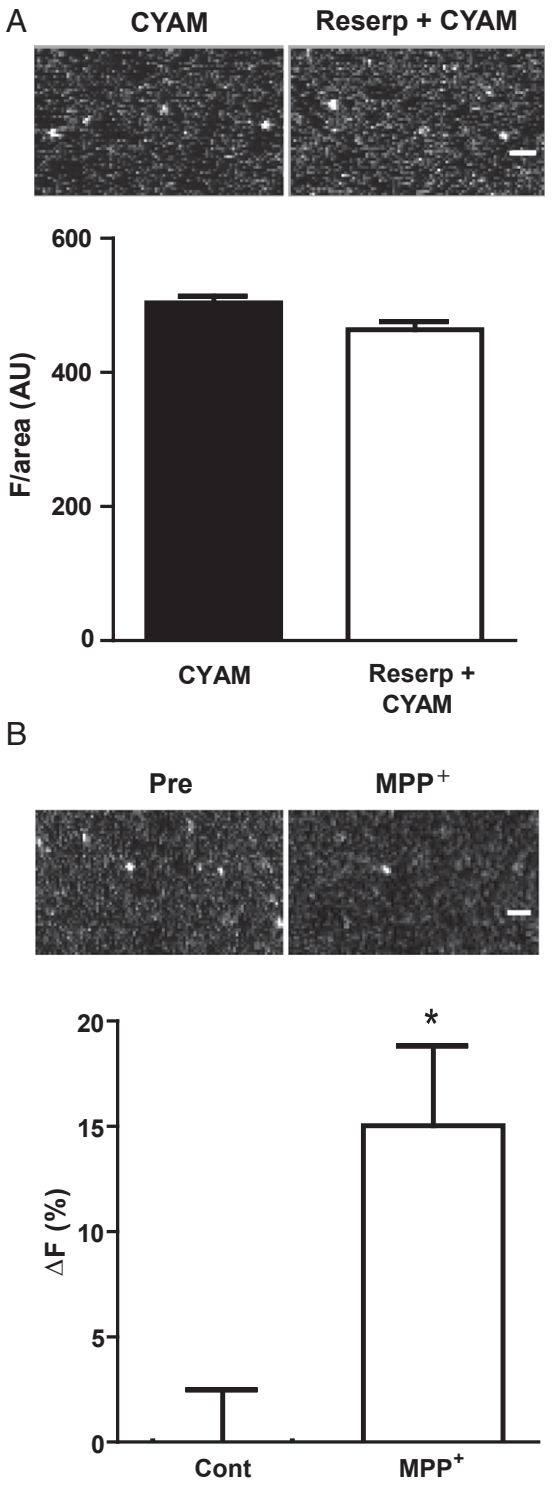

Fig. 9. VMAT does not affect CYAM accumulation, but mediates depletion. (*A*) CYAM accumulation is VMAT-independent. Striatum slices were pretreated with aCSF followed by CYAM treatment (control) or pretreated for 30 min with 500 nM reserpine followed by 1 h of coincubation with CYAM. (*Bottom*) Quantification of CYAM accumulation of six, 60 × 60-μm images per treatment is displayed as mean ± SEM. (*B*) MPP^+, a positively charged VMAT substrate, mimics pCA-induced changes in CYAM fluorescence. 2P image of CYAM-treated striatum slice treated with 50 μM MPP^+ for 20 min. (*Bottom*) Quantification of the change in CYAM fluorescence with MPP^+ treatment (n = 4–7 slices per treatment). (Scale bars: 2 μm.) *$P < 0.05$.

The slices were then held at room temperature until use. Subsequently, 0.005 μM CYAM, 0.1 μM CYAM, and 1 μM CYAM were incubated with tissue for 1 h and 3 h at 37 °C for concentration response experiments. For in vivo administration, CYAM in 0.9% sterile saline was injected i.p. twice daily at a dose of 2.5 mg/kg starting on postnatal day 14. Striatum slices were made 3 h after the morning dose on the first day (3 h) and then 48 h and 120 h later.

HA-DAT Immunohistochemistry. Striatum slices from HA-DAT mice (12) were prepared as above. Because the HA epitope in these animals is extracellular, no fixation or permeabilization was required. Slices were rinsed three times in room temperature aCSF, followed by a 1-h incubation at 37 °C with mouse anti-HA.11, clone 16B12 (BioLegend), at 1:250 in aCSF. The slices were then rinsed three more times with aCSF at room temperature for 5 min each time. The secondary antibody, Cy5 donkey anti-mouse Fab (Jackson ImmunoResearch Laboratories), was used at 1:100 in aCSF with 5 μM CYAM and was incubated with the tissue at room temperature for 1 h. Unbound antibody was then removed with three 5-min washes in aCSF at room temperature. The live slices were then held at room temperature in 5 μM CYAM in aCSF until use.

Imaging. Multiphoton imaging experiments were conducted on an Olympus Fluoview FV1000 upright confocal scanning microscope equipped with a Coherent Chameleon Ultra titanium/sapphire laser. The excitation light was attenuated with an acoustical optical modulator and expanded with a motorized telescope (LSM Technologies) before being focused with an Olympus LUMPlanFLN 60×, 1.0-W water immersion objective. CYAM has a reported emission spectrum of 450–675 nm, with a peak around 550 nm (5). The emission spectrum of Cy5 is 640–770 nm, with a peak at 665 nm. The emission beam was split with a T635LPxr dichroic mirror, and the CYAM signal was passed through a FF01-535/150 band-pass filter to a cooled gallium arsenide phosphide photomultiplier tube (PMT) (Hamamatsu Photonics). The Cy5 signal was passed through an HQ679/60m filter to a cooled bialkali Hamamatsu Photonics PMT. Both PMTs were used in conjunction with a nondescanned detector (LSM Technologies).

To determine the multiphoton excitation spectrum for CYAM, 50 mM CYAM in DMSO was diluted to 2 mM in pH 5, pH 6, and pH 7 phosphate-citrate buffer. Although peak fluorescence was between 740 and 750 nm, slice imaging used an excitation wavelength of 780 nm to minimize background and to excite both CYAM and Cy5. To determine the number of photons it takes to excite a CYAM molecule with 780 nm of light, 2 mM CYAM in phosphate-citrate buffer, pH 5, was excited with increasing laser power. The log of the resulting fluorescence intensity was plotted against the log of the laser power, and the slope was found by linear regression.

For experiments in which HA-DAT was labeled with the Cy5 Fab secondary, confocal microscopy was used for figure images due to the low multiphoton signal of the Cy5 Fab. A single-photon excitation wavelength of 635 nm was used for Cy5 Fab. CYAM was excited with 2P excitation and imaged as above. The 2P CYAM and 1P Cy5 images were then aligned with the "align slices in stack" plug-in from the MacBiophotonics suite of plug-ins (www.macbiophotonics.ca/software.htm) for ImageJ (NIH; imagej.nih.gov/ij/).

In experiments for which it was important to localize CYAM puncta to monoaminergic neurons, the fluorescent monoamine transporter substrate, IDT307 (also known as APP^+) was used (7–9). IDT307 has a wide 2P excitation spectrum ranging from ∼700–950 nm, with a peak at 870 nm (8). Its emission spectrum also overlaps with the emission spectrum of CYAM, at 450–600 nm (8). To eliminate the problem of overlap, 2P images of CYAM fluorescence were taken before a 10-min application of 0.5–1 μM IDT307 (a generous gift from Randy Blakely, Vanderbilt University, Nashville, TN). The 2P images of IDT307 were then taken with an excitation wavelength between 850 nm and 910 nm to reduce the overlap between IDT307 and CYAM signals further.

In all imaging experiments, data were acquired at 10 μs per pixel and had an axial spacing of 1.5 μm, and experiments were performed at room temperature. The stacks from before (pre)- and after (post)-stimulation/treatment were then compared by visual inspection relying on anatomical landmarks (cell bodies, nuclei, and vessels) to choose single optical sections from each stack that represent the same focal plane before and after treatment. In the striatum, only a single optical plane per time point was analyzed. However, in the SNc, the three central optical sections of a soma were summed using the "Z-projection" plug-in from the MacBiophotonics suite of plug-ins for ImageJ. Prestimulation- and poststimulation-summed stacks of somas were then aligned with the "align slices in stack" plug-in from the MacBiophotonics suite of plug-ins for ImageJ.

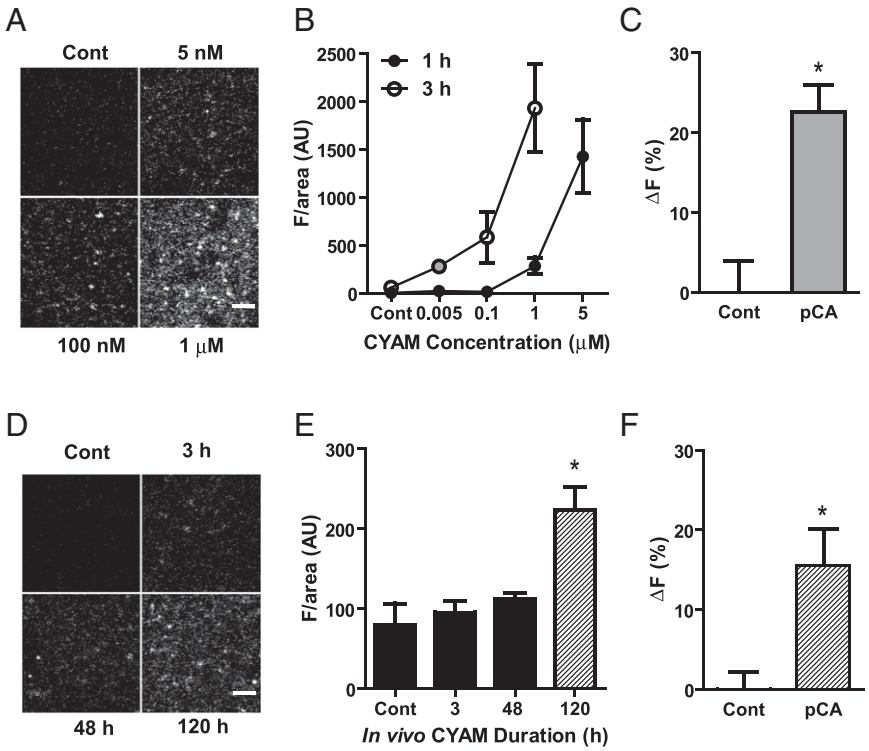

Fig. 10. In vitro and in vivo VMAT vesicular trapping of clinically relevant doses of CYAM. (*A* and *B*) Striatum slices were incubated for 1 or 3 h at 37 °C with 0, 0.005, 0.1, 1, and 5 μM CYAM. (*A*) Representative 2P images of slices treated for 3 h with CYAM at the concentrations indicated. (*B*) Concentration vs. fluorescence curves for 1 h (●; $n = 4$–5 slices per concentration) and 3 h (○; $n = 3$–13 slices per concentration) of incubation with CYAM at the concentrations indicated. (*C*) Change in CYAM fluorescence due to a 20-min application of 20 μM pCA or control in slices treated for 3 h with 5 nM CYAM ($n = 4$–7 slices). (*D* and *E*) For chronic in vivo CYAM treatment, striatum sections were collected from rats treated twice a day with a 2.5-mg/kg IP injection of CYAM, 3 h after the morning injection on the first (3 h), third (48 h), and sixth (120 h) days. Representative 2P images (*D*) and quantification of CYAM fluorescence of striatum slices (*E*) from rats chronically treated with CYAM ($n = 4$–5 slices per treatment). (*F*) Change in CYAM fluorescence due to a 20-min application of 20 μM pCA or control in slices from rats after 120 h of in vivo CYAM treatment ($n = 4$–5 slices per treatment). *$P < 0.05$. vs. control. (Scale bars: *A* and *C*, 5 μm.)

Electrophysiology. Patch electrodes were fabricated from Corning 7056 Patch Glass (Warner Instruments) and coated near the tip with beeswax to reduce the pipette capacitance (tip resistance of 4–6 MΩ). The pipette solution contained the following: 120 mM potassium gluconate, 20 mM KCl, 10 mM Hepes, 2 mM $MgCl_2$, 0.1 mM EGTA, and 1.2 mM ATP disodium salt (pH 7.3). Room temperature oxygenated aCSF was used for bath superfusion of midbrain slices at a rate of 2 mL·min^{-1}. Whole-cell current-clamp recordings were performed using a CV201A head stage, an Axopatch 200A Integrating Patch-Clamp amplifier, a DigiData 1322A 16-bit Data Acquisition System, and PClamp 10 software (Molecular Devices). Neurons of the SNc were filled via the whole-cell recording configuration through the patch pipette with 10 μM sulfo-Cy5-carboxylic acid (Lumiprobe Corporation) in pipette solution during recording. DA neurons were identified by well-defined electrophysiological characteristics [i.e., the presence of a sag in membrane potential upon hyperpolarization, spontaneous pacemaker-like activity of 1–10 Hz, broad (2–3 ms) action potentials] (29). Upon breakthrough to the whole-cell configuration, spontaneous activity was monitored for slow pacemaker activity. Action potential width and firing frequency were measured from these spontaneous recordings. To test for Ih sag potential, the neuron was current-clamped to −60 mV with bias current to prevent spontaneous activity, followed by a 4-s, −250-pA current injection. In experiments for CYAM localization in DA neurons, multiphoton microscopy images of CYAM and Cy5 fluorescence were taken in stacks of ten to fourteen 1.5-μm z-plane sections simultaneously after 5–10 min of Cy5 dialysis.

For electrical stimulation experiments in electrophysiologically defined DA neurons of the SNc, the cell was held at −60 mV with bias current and a prestimulation multiphoton image was taken for both CYAM and Cy5 simultaneously (as described above). The cell was then stimulated via patch pipette with twelve 10-s sweeps of 250- to 500-pA, 10- to 20-ms pulses (depending on what was needed to elicit reliable APs with each stimulation) at a frequency of 10 Hz with an intersweep interval of 10 s. The poststimulation image was taken with the same settings as the prestimulation image for both CYAM and Cy5.

Baf A and NH_4Cl Experiments. Unloaded SNc and striatum slices were treated with aCSF alone or with 10 nM or 1 μM vacuolar H^+ ATPase inhibitor Baf A (Sigma–Aldrich) for 30 min at room temperature. Slices treated with aCSF only were then treated with either aCSF with 0.01% DMSO (negative control) or 5 μM CYAM (positive control). CYAM (5 μM) was added to both Baf A treatments. All slices were then incubated for 1 h at 37 °C. 2P CYAM fluorescence was then compared across all treatments. To explore retention, SNc and striatum slices loaded with CYAM were treated with either aCSF or aCSF in which 5 mM NaCl was replaced with 5 mM NH_4Cl. During application, a 2P image of CYAM fluorescence was taken every 5 s for 60 s.

KCl Depolarization. In KCl depolarization experiments, SNc and striatum slices loaded with CYAM were pretreated for 10 min with aCSF (control), aCSF in which $CaCl_2$ was replaced with $MgCl_2$ and 1 mM EGTA was added (0 mM Ca^{2+}), or aCSF with 0.2 mM $CdCl_2$ added to block calcium channels (0.2 mM Cd^{2+}). The slice was then simulated for 2 min with either aCSF (time-matched control) or aCSF with 50 mM NaCl replaced with 50 mM KCl, 50 mM KCl and 0 mM Ca^{2+}, or 50 mM KCl and 0.2 mM Cd^{2+}.

Field Stimulation. In electrical field stimulation experiments, striatum slices loaded with CYAM were pretreated for 10 min with aCSF (control); 0 mM Ca^{2+}; 0.2 mM Cd^{2+}; or aCSF with 1 μM TTX, a voltage-gated sodium channel blocker (Alomone Labs). The slices were maintained in either control, 0 mM Ca^{2+}, 0.2 mM Cd^{2+}, or 1 μM TTX conditions while 2-ms-long pulses of 0 or 30 mA of current were passed between platinum electrodes placed on either side of the slice at a frequency of 10 Hz for 2 min.

pCA and MPP^+ Experiments. The pCA acts as a substrate for DAT, SERT, and VMAT to release DA and serotonin (10, 16, 30). Therefore, to determine if CYAM is in DA VMAT-expressing vesicles, combinations of DAT, SERT, and

VMAT inhibitors were coapplied with pCA. Striatum slices loaded with CYAM were pretreated for 5–10 min with aCSF (control); 10 μM GBR 12909 (Tocris), a DAT blocker; 1 μM nomifensine (Sigma–Aldrich), a DAT/norepinephrine transporter blocker; 10 μM fluoxetine (Sigma–Aldrich), a SERT inhibitor; or 500 nM reserpine (Sigma–Aldrich), a VMAT inhibitor. To each of these pretreatments, 20 μM pCA (Sigma-Aldrich) was added for 20 min. MPP^+ (50 μM; Sigma–Aldrich), a positively charged VMAT substrate, was applied to CYAM-loaded striatum slices for 20 min. To test whether blockade of VMAT by reserpine affects CYAM uptake, untreated striatum slices were pretreated with 500 nM reserpine for 30 min before coapplication of reserpine and CYAM for 1 h at 37 °C.

Analysis. Image analysis was performed with the MacBiophotonics suite of plug-ins for ImageJ. Pre- and posttreatment images were chosen and aligned as stated above (*Materials and Methods*, *Imaging*). For striatum slices, the pre-image was copied and the threshold function of ImageJ was used to create a mask from the top 3% brightest areas for rapid region of interest (ROI) selection. The "analyze particles" plug-in was then directed to use the mask ROI on both the pre- and post-images to measure mean fluorescence intensity per area, area, and raw intensity in arbitrary units, depending on the experiment. The process was similar for SNc soma CYAM fluorescence, except the ROI from the pre-image was created manually, excluding the nucleus. Both pre- and post-values were background-subtracted. The background fluorescence was measured in unloaded/empty cells, nuclei, or areas without structure. All ROIs were manually inspected, and those ROIs in which the puncta obviously moved or disappeared completely were discarded from analysis. However, post hoc analysis revealed that discarding such puncta had no effect, implying they made a minor contribution to the measurements. Similarly, some puncta got brighter. These ROIs were kept unless movement was obvious or the value was determined to be an outlier with Grubb's test for outliers.

Percent fluorescence change (ΔF) was calculated by the following equation:

$$\Delta F = [(\text{Pre} - \text{Post})/\text{Pre}] \times 100.$$

Therefore, a positive fluorescence change indicates a decrease in fluorescence. Fluorescence change values were also normalized to the change in the control experiments to allow comparison across experimental conditions.

Analysis of the NH_4Cl experiment was performed using the "Plot Profile" function of ImageJ. For puncta in SNc cell bodies (single optical plane, not summed) and striatum, the line tool was used to select the region through which to measure the fluorescence intensity profile. Those intensities were then plotted as a function of position, before and after treatment.

All values reported throughout this paper are the mean ± SEM. For striatum, an average ΔF of all puncta within a 60 × 60-μm area of a slice was calculated, and the mean ΔF of those slices is reported here. Therefore, for striatum data, *n* represents the number of slices per treatment, and for SNc, *n* represents the number of soma per treatment. Statistical significance was determined with paired *t* tests or, when there were multiple experimental groups, one-way ANOVA followed by a Dunnett's multiple comparison post hoc test in which the treatments were compared with a single control condition.

ACKNOWLEDGMENTS. We thank Dr. Alexander Sorkin for his comments on this manuscript. This research was supported by NIH Grant R21DA038384 (to E.S.L.), NIH Grant F32NS078994 (to K.R.T.), and NIH Grant R01DA014204 (to A. Sorkin, University of Pittsburgh, which supported E.R.B.).

1. Strange PG (2008) Antipsychotic drug action: Antagonism, inverse agonism or partial agonism. *Trends Pharmacol Sci* 29(6):314–321.
2. Dean B, Scarr E (2004) Antipsychotic drugs: Evolving mechanisms of action with improved therapeutic benefits. *Curr Drug Targets CNS Neurol Disord* 3(3):217–225.
3. Rayport S, Sulzer D (1995) Visualization of antipsychotic drug binding to living mesolimbic neurons reveals D2 receptor, acidotropic, and lipophilic components. *J Neurochem* 65(2):691–703.
4. Tischbirek CH, et al. (2012) Use-dependent inhibition of synaptic transmission by the secretion of intravesicularly accumulated antipsychotic drugs. *Neuron* 74(5):830–844.
5. Morlière P, et al. (2004) An insight into the mechanisms of the phototoxic response induced by cyamemazine in cultured fibroblasts and keratinocytes. *Photochem Photobiol* 79(2):163–171.
6. Limones-Herrero D, Pérez-Ruiz R, Jiménez MC, Miranda MA (2014) Retarded photooxidation of cyamemazine in biomimetic microenvironments. *Photochem Photobiol* 90(5):1012–1016.
7. Beikmann BS, Tomlinson ID, Rosenthal SJ, Andrews AM (2013) Serotonin uptake is largely mediated by platelets versus lymphocytes in peripheral blood cells. *ACS Chem Neurosci* 4(1):161–170.
8. Karpowicz RJ, Jr, Dunn M, Sulzer D, Sames D (2013) APP+, a fluorescent analogue of the neurotoxin MPP+, is a marker of catecholamine neurons in brain tissue, but not a fluorescent false neurotransmitter. *ACS Chem Neurosci* 4(5):858–869.
9. Chang JC, et al. (2012) Single molecule analysis of serotonin transporter regulation using antagonist-conjugated quantum dots reveals restricted, p38 MAPK-dependent mobilization underlying uptake activation. *J Neurosci* 32(26):8919–8929.
10. Sharp T, Zetterström T, Christmanson L, Ungerstedt U (1986) p-Chloroamphetamine releases both serotonin and dopamine into rat brain dialysates in vivo. *Neurosci Lett* 72(3):320–324.
11. Rodriguez PC, et al. (2013) Fluorescent dopamine tracer resolves individual dopaminergic synapses and their activity in the brain. *Proc Natl Acad Sci USA* 110(3):870–875.
12. Rao A, Richards TL, Simmons D, Zahniser NR, Sorkin A (2012) Epitope-tagged dopamine transporter knock-in mice reveal rapid endocytic trafficking and filopodia targeting of the transporter in dopaminergic axons. *FASEB J* 26(5):1921–1933.
13. Wall SC, Gu H, Rudnick G (1995) Biogenic amine flux mediated by cloned transporters stably expressed in cultured cell lines: Amphetamine specificity for inhibition and efflux. *Mol Pharmacol* 47(3):544–550.
14. Sulzer D, Rayport S (1990) Amphetamine and other psychostimulants reduce pH gradients in midbrain dopaminergic neurons and chromaffin granules: A mechanism of action. *Neuron* 5(6):797–808.
15. Sulzer D, St Remy C, Rayport S (1996) Reserpine inhibits amphetamine action in ventral midbrain culture. *Mol Pharmacol* 49(2):338–342.
16. Partilla JS, et al. (2006) Interaction of amphetamines and related compounds at the vesicular monoamine transporter. *J Pharmacol Exp Ther* 319(1):237–246.
17. Sulzer D, et al. (1995) Amphetamine redistributes dopamine from synaptic vesicles to the cytosol and promotes reverse transport. *J Neurosci* 15(5 Pt 2):4102–4108.
18. Sulzer D, Maidment NT, Rayport S (1993) Amphetamine and other weak bases act to promote reverse transport of dopamine in ventral midbrain neurons. *J Neurochem* 60(2):527–535.
19. Sulzer D, et al. (1992) Weak base model of amphetamine action. *Ann N Y Acad Sci* 654:525–528.
20. Eiden LE, Schäfer MK, Weihe E, Schütz B (2004) The vesicular amine transporter family (SLC18): Amine/proton antiporters required for vesicular accumulation and regulated exocytotic secretion of monoamines and acetylcholine. *Pflugers Arch* 447(5):636–640.
21. Hyland BI, Reynolds JNJ, Hay J, Perk CG, Miller R (2002) Firing modes of midbrain dopamine cells in the freely moving rat. *Neuroscience* 114(2):475–492.
22. Sulzer D, Sonders MS, Poulsen NW, Galli A (2005) Mechanisms of neurotransmitter release by amphetamines: A review. *Prog Neurobiol* 75(6):406–433.
23. Knoth J, Peabody JO, Huettl P, Njus D (1984) Kinetics of tyramine and permeation across cromaffin-vesicle membranes. *Biochemistry* 23(9):2011–2016.
24. Romanenko VG, Gebara R, Miller KM, Njus D (1998) Determination of transport parameters of permeant substrates of the vesicular amine transporter. *Anal Biochem* 257(2):127–133.
25. Shepard PD, Canavier CC, Levitan ES (2007) Ether-a-go-go-related gene potassium channels: What's all the buzz about? *Schizophr Bull* 33(6):1263–1269.
26. Ji H, et al. (2012) Functional characterization of ether-à-go-go-related gene potassium channels in midbrain dopamine neurons—Implications for a role in depolarization block. *Eur J Neurosci* 36(7):2906–2916.
27. Tucker KR, Huertas MA, Horn JP, Canavier CC, Levitan ES (2012) Pacemaker rate and depolarization block in nigral dopamine neurons: A somatic sodium channel balancing act. *J Neurosci* 32(42):14519–14531.
28. Putzier I, Kullmann PH, Horn JP, Levitan ES (2009) Cav1.3 channel voltage dependence, not Ca2+ selectivity, drives pacemaker activity and amplifies bursts in nigral dopamine neurons. *J Neurosci* 29(49):15414–15419.
29. Ungless MA, Grace AA (2012) Are you or aren't you? Challenges associated with physiologically identifying dopamine neurons. *Trends Neurosci* 35(7):422–430.
30. Rudnick G, Wall SC (1992) p-Chloroamphetamine induces serotonin release through serotonin transporters. *Biochemistry* 31(29):6710–6718.